ChemComm

COMMUNICATION

View Article Online
View Journal | View Issue

Cite this: *Chem. Commun.*, 2025, **61**, 4836

Received 8th February 2025,
Accepted 27th February 2025

DOI: 10.1039/d5cc00688k

rsc.li/chemcomm

Solvent-mediated subcomponent self-assembly of covalent metallacycles for hierarchical porous materials synthesis†

Zhi-Wei Li, *[ab] Anlian Huang,[b] Zhenguo Wang,[ab] Rui Gao,[ab] Bang Lan,*[a] Guosheng Chen *[b] and Gangfeng Ouyang[b]

We report a solvent-mediated subcomponent self-assembly strategy for synthesizing tetranuclear and triangular covalent metallacycles. The results demonstrate that the polarity of solvent significantly influences the structural outcome of metallacycles, and the square-shaped metallacycles can serve as building blocks for the construction of hierarchical porous materials such as metallacycle-based hydrogen-bonded organic frameworks (mHOFs) and metal–organic frameworks (mMOFs).

Since the groundbreaking synthesis of crown ethers by C. J. Pedersen,[1] the field of covalent macrocycles has garnered extensive research interest.[2–4] Over the past decades, a wide variety of covalent macrocycles, such as cyclodextrin,[5] calixarene,[6] and cyclophane,[7] have been synthesized and have seen extensive applications in fields including molecular recognition,[8] adsorption,[9] and catalysis.[10] These classical covalent macrocycles are linked by irreversible covalent bonds, making their synthesis a kinetically controlled process that typically yields lower quantities.[11] In this context, various types of reversible and dynamic covalent bonds, such as imine,[12] borate,[13] olefin,[14] and disulfide linkages,[15] have been employed to synthesize covalent macrocycles, generally achieving nearly quantitative yields. Nevertheless, even subtle alterations in the structure of the building blocks can lead to an inability to synthesize the desired macrocyclic compounds.[16] Thus, the modular synthesis of macrocyclic molecules with precise structures and tailored functions continues to pose a significant challenge.

Furthermore, covalent macrocycles can also serve as building blocks for the synthesis of hydrogen-bonded organic frameworks (HOFs),[17,18] metal–organic frameworks (MOFs),[19] and covalent organic frameworks (COFs).[20] The inherent cavities of covalent macrocycles endow these macrocycle-based materials with hierarchical structures. For example, Hisaki, Miyata, and co-workers reported on a series of C_3-symmetric covalent macrocycles that incorporate multiple carboxylic acid groups, which are utilized in the construction of HOFs.[21] Similarly, Cui, Farha, and their research team utilized covalent macrocycle containing carboxylic groups to synthesize zirconium-based MOFs.[22] However, the synthesis of these covalent macrocycles requires multiple steps and ultimately results in low yields. In our recent research, we have developed an efficient method for constructing covalent metallacycles (**CMs**).[23] This approach utilizes a one-pot subcomponent self-assembly technique, leveraging metal centers as the templates, 2,6-diacetylpyridine or its derivatives as the corners, and terephthalic dihydrazide (**THA**) as the edges to synthesize tetranuclear **CMs** with high yields. Importantly, task-specific, custom-tailored **CMs** can be readily accessible by modifying the structure of their corners and edges. Considering the shape and rigid framework of these **CMs**, we anticipate that they could serve as foundational building blocks for the synthesis of macrocycle-based materials. The assembly mode of these **CMs** can be precisely controlled by altering the functional groups surrounding them.

In this study, we describe the synthesis of covalent metallacycles *via* subcomponent self-assembly in different solvents (Scheme 1). The results show that the solvent polarity plays a critical role in dictating the structural outcome of the metallacycles. Specifically, the use of CH_3OH and DMF, both polar solvents, predominantly yields tetranuclear metallacycles, whereas the more polar solvent DMSO facilitates the formation of a mixture of tetranuclear and triangular metallacycles. Using the square tetranuclear metallacycles as building blocks, two different types metallacycle-based materials were successfully obtained through different assembling strategies.

[a] *Northeast Guangdong Key Laboratory of New Functional Materials, School of Chemistry and Environment, Jiaying University, Meizhou, 514015, China. E-mail: lizhw69@mail.sysu.edu.cn, jyulb6@163.com*
[b] *MOE Key Laboratory of Bioinorganic and Synthetic Chemistry, GBRCE for Functional Molecular Engineering, School of Chemistry, IGCME, Sun Yat-Sen University, Guangzhou, 510275, China. E-mail: chengsh39@mail.sysu.edu.cn*

† Electronic supplementary information (ESI) available. CCDC 2415029. For ESI and crystallographic data in CIF or other electronic format see DOI: https://doi.org/10.1039/d5cc00688k

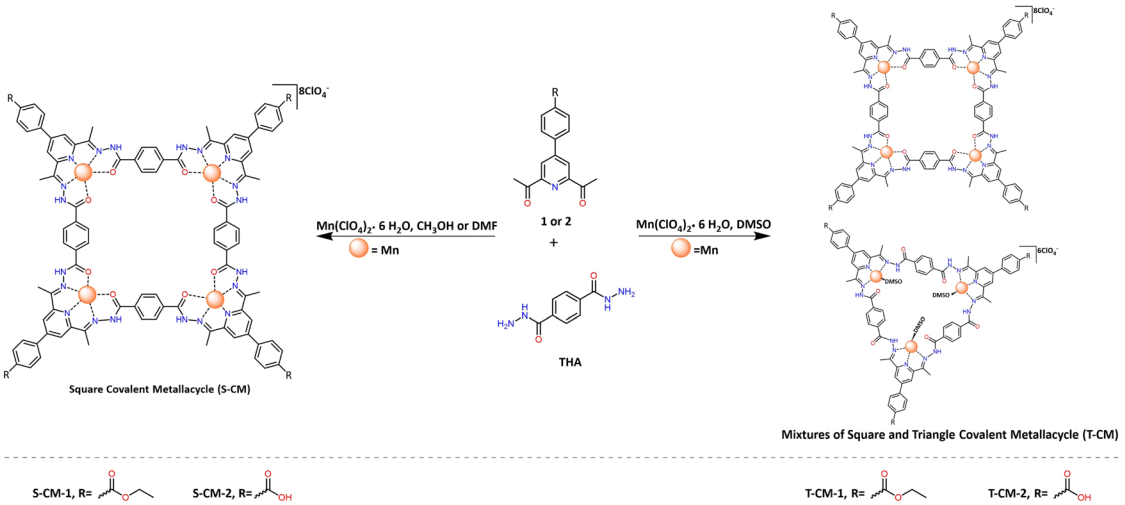

Scheme 1 Solvent-mediated synthesis of square covalent metallacycle (**S-CM**) and triangle covalent metallacycle (**T-CM**) *via* one-pot subcomponent self-assembly. The axially coordinated solvent molecules in **S-CM** are omitted for clarity.

First, ligand **1** was synthesized through a Suzuki cross-coupling reaction between 4-bromo-2,6-diacetylpyridine and 4-dihydroxyboranyl-benzoic acid ethyl ester with a good yield (Scheme S1 and Fig. S1–S3, ESI†). Subsequent hydrolysis of ligand **1** resulted in ligand **2** (Scheme S1 and Fig. S4, S5, ESI†). Both the ethyl ester[24] and carboxylic acid groups have the potential to engage in hydrogen bonding, with the carboxylic acid groups also being capable of coordinating with metal ions. Moreover, the inclusion of benzene rings in ligands **1** and **2** not only offers additional interaction sites for the assembly of the desired **CMs** but also enhances the freedom of the peripheral ethyl ester and carboxyl groups.

Following our previous method, a one-pot reaction of ligand **1**, **THA**, and Mn $(ClO_4)_2{\cdot}6H_2O$ in an identical molar ratio in CH_3OH yielded a yellow solution and given a yellow product at an almost quantative yield after removing the solvent. High-resolution electrospray ionization mass spectrometry (HRESI-MS) analysis of the resulting solid confirmed the successful formation of a tetranuclear complex (**S-CM-1′**). The peaks found at *m*/*z* = 418.8864, *m*/*z* = 523.3561 and *m*/*z* = 697.4718 were identified to the chemical compositions of $[C_{104}H_{89}N_{20}O_{16}Mn_4]^{5+}$, $[C_{104}H_{88}N_{20}O_{16}Mn_4]^{4+}$, $[C_{104}H_{87}N_{20}O_{16}Mn_4]^{3+}$, respectively (Fig. S6, ESI†). The isotopic distribution obtained by the experiment is in good agreement with the simulated one (Fig. S7, ESI†). The slow diffusion of pyridine vapor into the a dimethylformamide (DMF) solution of **S-CM-1′** led to block-shaped crystals (Fig. S16, ESI†) suitable for single-crystal X-ray diffraction (SCXRD). SCXRD analysis revealed that the crystals are assembled from deprotonated square covalent metallacycles, crystallizing in the $P\bar{1}$ space group (**S-CM-1**, Table S1, ESI†). The highly disordered solvent molecules including DMF and pyridine were removed using the solvent masking procedure (Fig. S17, ESI†).[25] The distance between adjacent ethyl ester groups is up to 3 nm (Fig. 1a). The Mn^{2+} ions coordinate with five N_3O_2 atoms in the equatorial plane, and two pyridine molecules at the axial positions, respectively. The metallacycles are arranged near each other through π···π interactions between the axially coordinated

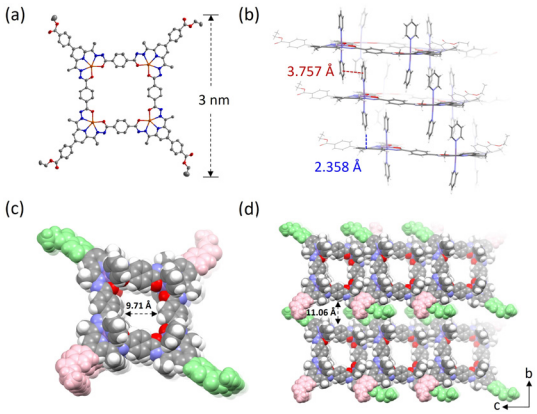

Fig. 1 (a) X-ray crystal structure of **S-CM-1** with 50% thermal ellipsoids, the axially coordinated pyridine molecules and hydrogen atoms are omitted for clarity. Color code: C = gray, N = blue, O = red, Mn = orange. (b) π···π (red dash line) and H···π (blue dash line) interactions between the metallacycles. (c) 1D channel formed by metallacycles stacking. (d) The 3D framework with two types of channels viewed along *a* axis.

pyridine molecules, as well as H···π interactions between these pyridine molecules and the pyridyl moieties within the metallacycles (Fig. 1b). This arrangement forms a columnar channel with a diameter of 9.71 Å (Fig. 1c). The stacked metallacycles are further interconnected through various noncovalent interactions between the cross-stacked ethyl ester groups (Fig. S18 and Table S2, ESI†), leading to the formation of a porous, crystalline metallacycle-based material (Fig. 1d). Additionally, Hirshfeld surface analysis[26] was also perform to probe the noncovalent interactions in **S-CM-1**. Indeed, multiple intermolecular hydrogen bondings including C–H···O and C–H···N were found with the framework of **S-CM-1** (Fig. S19–S21, ESI†). The phase purity of **S-CM-1** powder was confirmed through powder X-ray diffraction analysis (Fig. S22, ESI†). Thermogravimetric experiments indicated that **S-CM-1** exhibits exceptional

thermal stability (Fig. S23, ESI†), likely attributed to the numerous noncovalent interactions within its framework.

Considering the poor solubility of ligand **2** in methanol, DMF was chosen as the solvent for the self-assemble reaction. A one-pot reaction of ligand **2**, **THA**, and Mn $(ClO_4)_2{\cdot}6H_2O$ in an equimolar ratio at 80 °C in DMF resulted in the successful formation of a tetranuclear metallacycle incorporating carboxyl groups (denoted as **S-CM-2**), which was confirmed by HRESI-MS analysis (Scheme S3 and Fig. S8, S9, ESI†). These findings indicate that DMF does not influence the formation process of metallacycle. Unfortunately, numerous attempts fail to obtain suitable single crystals of **S-CM-2** for SCXRD.

The formation of covalent metallacycles relies crucially on coordination bonds between metal ion templates and organic subcomponents, which are highly sensitive to changes in solvent polarity.[27] In this context, we turned attention to investigate the assembly behaviour of the subcomponents in dimethyl sulfoxide (DMSO), a more polar solvent than DMF. A reaction of ligand **1**, **THA**, and Mn $(ClO_4)_2{\cdot}6H_2O$ in an equimolar ratio in DMSO resulted in a clear yellow solution, which was directly used for HRESI-MS analysis. Surprisingly, in addition to the tetranuclear metallacycle, a [3+3] triangular dinuclear metallacycle was observed in the solution. As shown in Fig. S10 (ESI†), three peaks at m/z = 505.4653, m/z = 757.6934, and m/z = 796.7006 were assigned to the chemical compositions of $[C_{78}H_{68}N_{15}O_{12}Mn_2]^{3+}$, $[C_{78}H_{67}N_{15}O_{12}Mn_2]^{2+}$, $[C_{78}H_{67}N_{15}O_{12}Mn_2(DMSO)]^{2+}$, respectively (**T-CM-1**, Fig. S11, ESI†). While for the solution resulting from the assembly of ligand **2**, **THA**, and Mn $(ClO_4)_2{\cdot}6H_2O$, another [3+3] triangular trinuclear metallacycle was found (**T-CM-2**, Fig. 2 and Fig. S12, S13, ESI†). The peak at m/z = 547.0865 was identified to a chemical composition of $[C_{72}H_{54}N_{15}O_{12}Mn_3\ (DMSO)_2]^{3+}$ (Fig. 2b), suggesting that the Mn ions in the skeleton may coordinate with two DMSO molecules. These HRESI-MS results indicate that DMSO plays an important role in the formation of covalent metallacycles. Previous studies have revealed that the oxygen atoms of DMSO can also coordinate with Mn^{2+} ions.[28] We speculate that the formation of square and triangular mixtures arise from the dynamic and competitive coordination interactions between DMSO (C_2H_6S = O···Mn) and carbonyl oxygens (–C═O···Mn) with Mn^{2+} ions. As depicted in Fig. S24 (ESI†), a plausible formation mechanism for the square and triangular mixtures has been elucidated. The oligomeric $Mn_2THA_2L_3$ is a crucial intermediate for further cyclization into the square and triangular products. In $Mn_2THA_2L_3$, the coordination environment of Mn^{2+} ions are in a dynamic equilibrium between pentacoordinate MnN_3O_2 and tetradentate MnN_3(DMSO). The tetradentate coordination mode would lead to smaller angles between the linkages, ultimately condensing to form triangular metallacycles. Moreover, the one-pot assembly of Zn ions, **THA**, and ligand **1** in DMSO also produced a mixture of triangular and square metallacycles (Scheme S6 and Fig. S14, S15, ESI†), demonstrating the universality of our strategy.

Next, the C_4-symmetric **S-CM-2**, containing four carboxylic acid groups, was further reacted with $ZrOCl_2$ in the presence of benzoic acid as a modulator in DMF, resulting in a brown-yellow solid (Scheme 2). PXRD patterns of the resulting solid, when immersed in the mother liquor, confirm the successful formation of a crystalline metallacycle-based metal–organic framework (denoted as **mMOF-1**, Fig. 3a). The pronounced differences in the PXRD patterns of **mMOF-1**, when compared to those of typical Zr-based MOFs constructed from neutral C_4-symmetric ligands (Table S3 and Fig. S25, S26, ESI†), imply that the inherent positive charge of the **S-CM-2** ligand significantly influences its assembly with Zr_6 clusters. However, the solid powder after centrifugation and drying shows an amorphous state (Fig. S27, ESI†), suggesting that solvent molecules are essential for maintaining its crystalline structure. The insolubility of mMOF-1 in both DMF and DMSO indicates its polymeric nature (Fig. S28, ESI†). mMOF-1 also shows an exceptional thermal stability with a decomposition temperature up to 400 °C (Fig. S29, ESI†). Furthermore, scanning electron microscopy (SEM) was performed to investigated the morphology of amorphous **mMOF-1**. As shown in Fig. 3b, **mMOF-1** exhibits a cubic shape with smooth surfaces, even though it has lost its crystallinity. We also employed transmission electron microscopy (TEM) with energy dispersive X-ray spectra (EDS) to acquire elemental mappings at the microscopic level. The AC-HAADF-STEM results show a uniform distribution of Mn, Zr, and Cl elements throughout the cubic particles. It is worth mentioning that the presence of Cl element indicates the

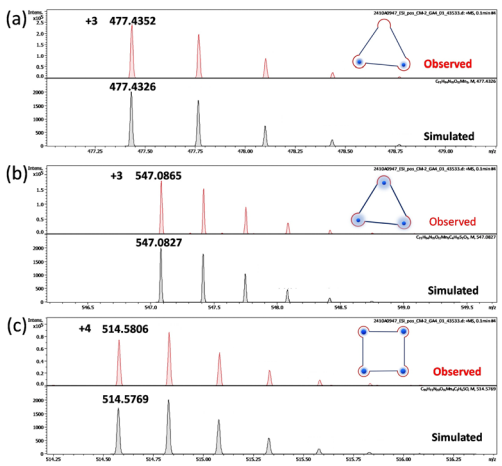

Fig. 2 The observed and simulated peaks found in the **S-CM-2** and **T-CM-2** mixtures. (a) $[C_{72}H_{56}N_{15}O_{12}Mn_2]^{3+}$, (b) $[C_{72}H_{54}N_{15}O_{12}Mn_3\ (DMSO)_2]^{3+}$, (c) $[C_{96}H_{72}N_{20}O_{16}Mn_4\ (DMSO)]^{4+}$.

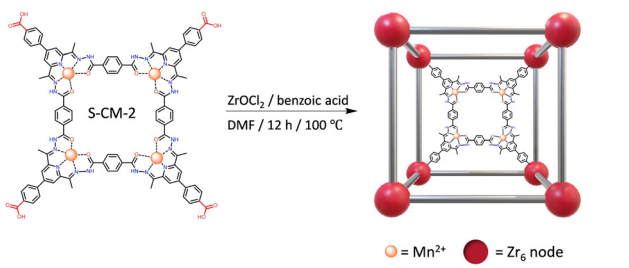

Scheme 2 Synthesis of the zirconium-based MOFs using **S-CM-2** as building blocks.

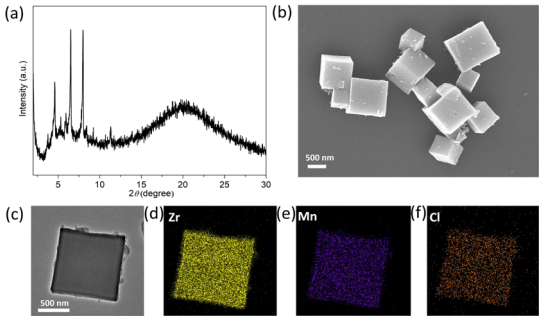

Fig. 3 (a) PXRD patterns of **mMOF-1**, (b) SEM image of **mMOF-1**, (c)–(f) AC-HAADF-STEM image and the corresponding EDS elemental mapping of **mMOF-1**.

presence of ClO_4^- within the framework, indicating that the whole framework is positively charged. X-ray photoelectron spectroscopy (XPS) analysis further determine the oxidation state of the Mn element to be +2 (Fig. S30 and S31, ESI†), remaining as the **S-CM-2**.

In summary, we have developed a modular and solvent-mediated assembly strategy for the construction of covalent metallacycles. By varying the building blocks, two square-shaped covalent metallacycles, containing ethyl ester groups (**S-CM-1**) and carboxyl groups (**S-CM-2**), were synthesized and characterized using HRESI-MS and SCXRD. **S-CM-1** is a metallacycle-based hydrogen-bonded organic framework, assembled from covalent metallacycles through multiple non-covalent interactions. While **S-CM-2** was chosen as a building block for the hierarchical assemble with $ZrOCl_2$, resulting the formation of a metallacycle-based metal–organic framework. Moreover, we also found that the choice of solvent significantly influences the shape of covalent metallacycles. In a highly polar DMSO solution, an unexpectedly triangular metallacycle was detected by HRESI-MS analysis. In addition, the modular synthesis strategy makes it easy to prepare metallacycles modified with different functional groups, especially amino and aldehyde groups, which can be used as building blocks to synthesize metallacycle-based frameworks. Given their abundant open metal sites[29,30] and hierarchically porous structures, these metallacycle-based frameworks are expected to exhibit exceptional performance in adsorption and catalysis.

This work was supported by the National Natural Science Foundation of China (22174164, 22336007) and Guangdong Basic and Applied Basic Research Foundation (2022A15150 10051, 2024B1515020070).

Data availability

The data supporting this article have been included as part of the ESI.† Crystallographic data for **S-CM-1** has been deposited at the CCDC under 2415029.†

Conflicts of interest

There are no conflicts to declare.

References

1 C. J. Pedersen and H. K. Frensdorff, *Angew. Chem., Int. Ed. Engl.*, 1972, **11**, 16–25.
2 Y. Qin, X. Liu, P.-P. Jia, L. Xu and H.-B. Yang, *Chem. Soc. Rev.*, 2020, **49**, 5678–5703.
3 Q. Liu, M. Zuo, K. Wang and X.-Y. Hu, *Chem. Commun.*, 2023, **59**, 13707–13710.
4 W. Chen, P. Chen, G. Zhang, G. Xing, Y. Feng, Y.-W. Yang and L. Chen, *Chem. Soc. Rev.*, 2021, **50**, 11684–11714.
5 Z. Liu and Y. Liu, *Chem. Soc. Rev.*, 2022, **51**, 4786–4827.
6 H. Ren, H. Wang, W. Wen, S. Li, N. Li, F. Huo and C. Yin, *Chem. Commun.*, 2023, **59**, 13790–13799.
7 T. Jiao, K. Cai, J. N. Nelson, Y. Jiao, Y. Qiu, G. Wu, J. Zhou, C. Cheng, D. Shen, Y. Feng, Z. Liu, M. R. Wasielewski, J. F. Stoddart and H. Li, *J. Am. Chem. Soc.*, 2019, **141**, 16915–16922.
8 F. A. Mohammed, T. Xiao, L. Wang and R. B. P. Elmes, *Chem. Commun.*, 2024, **60**, 11812–11836.
9 W. Zhou, R. Lavendomme and D. Zhang, *Chem. Commun.*, 2024, **60**, 779–792.
10 Q.-Q. Wang, *Acc. Chem. Res.*, 2024, **57**, 3227–3240.
11 C. Storz, M. Badoux, C. M. Hauke, T. Šolomek, A. Kühnle, T. Bally and A. F. M. Kilbinger, *J. Am. Chem. Soc.*, 2014, **136**, 12832–12835.
12 T. Jiao, G. Wu, Y. Zhang, L. Shen, Y. Lei, C.-Y. Wang, A. C. Fahrenbach and H. Li, *Angew. Chem., Int. Ed.*, 2020, **59**, 18350.
13 R. Nishiyabu, Y. Kubo, T. D. James and J. S. Fossey, *Chem. Commun.*, 2011, **47**, 1124–1150.
14 V. H. Gessner, J. F. Tannaci, A. D. Miller and T. D. Tilley, *Acc. Chem. Res.*, 2011, **44**, 435–446.
15 S. Otto, *Acc. Chem. Res.*, 2022, **55**, 145–155.
16 L. Shen, N. Cao, L. Tong, X. Zhang, G. Wu, T. Jiao, Q. Yin, J. Zhu, Y. Pan and H. Li, *Angew. Chem., Int. Ed.*, 2018, **57**, 16486.
17 H. Wang, D. Wang, Y. Wu and Y. Zhao, *Chem. – Eur. J.*, 2024, **30**, e202303618.
18 Z.-W. Li, Z.-J. Huang, Y.-X. Li, X. Wu, W. Shi, Y.-B. Zhang, X. Ma, G. Ouyang, B.-H. Ye, G.-F. Liu and X.-M. Chen, *CCS Chem.*, 2025, **7**, 293–306.
19 T.-H. Chen, I. Popov, Y.-C. Chuang, Y.-S. Chen and O. Š. Miljanić, *Chem. Commun.*, 2015, **51**, 6340–6342.
20 H. Yang, Y. Du, S. Wan, G. D. Trahan, Y. Jin and W. Zhang, *Chem. Sci.*, 2015, **6**, 4049–4053.
21 I. Hisaki, S. Nakagawa, N. Ikenaka, Y. Imamura, M. Katouda, M. Tashiro, H. Tsuchida, T. Ogoshi, H. Sato, N. Tohnai and M. Miyata, *J. Am. Chem. Soc.*, 2016, **138**, 6617–6628.
22 W. Gong, Y. Xie, X. Wang, K. O. Kirlikovali, K. B. Idrees, F. Sha, H. Xie, Y. Liu, B. Chen, Y. Cui and O. K. Farha, *J. Am. Chem. Soc.*, 2023, **145**, 2679–2689.
23 Z.-W. Li, X. Wang, L.-Q. Wei, I. Ivanović-Burmazović and G.-F. Liu, *J. Am. Chem. Soc.*, 2020, **142**, 7283–7288.
24 Q. Huang, X. Chen, W. Li, Z. Yang, Y. Zhang, J. Zhao and Z. Chi, *Chemistry*, 2023, **9**, 1241–1254.
25 A. L. Spek, *Acta Crystallogr., Sect. C: Cryst. Struct. Commun.*, 2015, **C71**, 9–18.
26 M. A. Spackman and D. Jayatilaka, *CrystEngComm*, 2009, **11**, 19–32.
27 H. Kurz, P. C. P. Teeuwen, T. K. Ronson, J. B. Hoffman, P. Pracht, D. J. Wales and J. R. Nitschke, *J. Am. Chem. Soc.*, 2024, **146**, 30958–30965.
28 E. Szostak, A. Migdał-Mikuli, A. Kaczor and W. Nitek, *Spectrochim. Acta, Part A*, 2011, **79**, 1179–1186.
29 Z.-Q. Lin, S.-L. Zheng, J. Hu, H.-Q. Zhou, Z. Feng, Y. He, L.-H. Chung and J. He, *J. Mater. Chem. C*, 2021, **9**, 10288–10294.
30 H. Zhong, Z. Jiang, J. Hu, L.-H. Chung and J. He, *Chem. Commun.*, 2024, **60**, 7578–7581.